Protected Nodal Electron Pocket from Multiple-Q Ordering in Underdoped High Temperature Superconductors

N. Harrison[1] and S. E. Sebastian[2]

[1]National High Magnetic Field Laboratory, Los Alamos National Laboratory, MS E536, Los Alamos, New Mexico 87545, USA
[2]Cavendish Laboratory, Cambridge University, JJ Thomson Avenue, Cambridge CB3 OHE, United Kingdom

(Received 8 March 2011; published 31 May 2011)

A multiple wave vector (**Q**) reconstruction of the Fermi surface is shown to yield a profoundly different electronic structure to that characteristic of single wave vector reconstruction, despite their proximity in energy. We consider the specific case in which ordering is generated by $\mathbf{Q}_x = [2\pi a, 0]$ and $\mathbf{Q}_y = [0, 2\pi b]$ (in which $a = b = \frac{1}{4}$)—similar to those identified in neutron diffraction and scanning tunneling microscopy experiments—and more generally show that an isolated pocket adjacent to the nodal point $\mathbf{k}_{\text{nodal}} = [\pm\frac{\pi}{2}, \pm\frac{\pi}{2}]$ is a protected feature of such a multiple-**Q** model, potentially corresponding to the nodal "Fermi arcs" observed in photoemission and the small size of the electronic heat capacity found in high magnetic fields—importantly, containing electron carriers which can yield negative Hall and Seebeck coefficients observed in high magnetic fields.

DOI: 10.1103/PhysRevLett.106.226402 PACS numbers: 71.18.+y, 71.45.Lr, 74.25.Jb, 75.40.Mg

It has been challenging to identify the origin of small Fermi surface (FS) pockets observed by quantum oscillations in underdoped $YBa_2Cu_3O_{6+x}$ [1–4], given the absence of a unique expectation for the electronic structure from theoretical predictions in this regime [5]. While the details of the ordering differs between models, all translational symmetry-breaking models proposed thus far involve a single translational vector **Q** [6] causing them to yield FS topologies with the same universal features—hole pockets and/or open sheets at the nodal point $\mathbf{k}_{\text{nodal}} = [\pm\frac{\pi}{2}, \pm\frac{\pi}{2}]$ in the extended Brillouin zone (BZ) and the possibility of an electron pocket at the antinodal point $\mathbf{k}_{\text{antinodal}} = [\pi, 0]$ and $[0, \pi]$. It becomes important to search for new models outside the realm of these universal features, which have difficulty simultaneously capturing the high field negative Hall and Seebeck coefficients [2] (interpreted in terms of an antinodal electron pocket [6]) and the pseudogap at the same location in zero field observed by angle-resolved photoemission spectroscopy (ARPES) and scanning tunneling microscopy (STM) [7–9]. While it has been suggested that translational symmetry-breaking models may be relevant only in the high magnetic field regime of quantum oscillations, experiments have yet to establish the effect of a field in changing the electronic structure [10,11].

Here we introduce a new possibility which we suggest is more applicable to the experimental situation in the underdoped cuprates. We show that multiple-**Q** ordering yields a FS consisting of a protected electron pocket at the nodes—rather surprisingly, while the multiple-**Q** charge ordering solution is argued to be close in energy to the single-**Q** charge ordering solution [12], the consequences for electronic structure are profoundly different. In the case of underdoped $YBa_2Cu_3O_{6+x}$, a single electron pocket at the nodes produced by a range of coupling strengths in this model is most consistent with the single type of carrier pocket revealed by chemical potential quantum oscillations [13] and the density of states concentrated chiefly at the nodes in ARPES [7,8] and in-field heat capacity experiments [11]; indeed, the electron character of this pocket also yields negative Hall and Seebeck coefficients as experimentally observed [2]. We consider the case in which two orthogonal vectors $\mathbf{Q}_x = [2\pi a, 0]$ and $\mathbf{Q}_y = [0, 2\pi b]$ with $a \approx b \approx \frac{1}{4}$ lead to a $\approx$ 16-fold reduction in the size of the BZ. Despite the aggregation of holes at $\mathbf{k}_{\text{nodal}}$ in the extended BZ, their density exceeds 50% of the reconstructed BZ cross section at the dopings relevant for quantum oscillation studies [1,2]—the electron pocket resulting from a >50% filling of the folded band with holes. Unlike the antinodal electron pocket predicted by single-**Q** models [6], the electron pocket found here incorporates the nodal "arc" region of the FS (see Fig. 1) seen in ARPES [7,8].

Evidence for ordering at wave vectors $\mathbf{Q}_x$ and $\mathbf{Q}_y$ is found in neutron diffraction [14] and STM [15,16] measurements, with the possibilities including domains of unidirectional spin or charge stripes [17], stripes alternating on consecutive layers [18], or multiple-**Q** charge ordering without a static spin component [7,16,19]. The latter may be relevant in underdoped $YBa_2Cu_3O_{6+x}$, where neutron scattering experiments find evidence for quasistatic spin ordering at oxygen compositions ($x < 0.45$, corresponding to hole dopings $\delta \lesssim 8\%$) lower than those in which quantum oscillations are observed [20], while charge ordering is observed at the same and higher dopings (orthogonal [21] and parallel [22] to the chain direction). Furthermore, the observation of spin zeros in magnetic quantum oscillation experiments is more easily explained by a scenario involving long-range ordering of only the charge degrees of freedom [4].

We show in Fig. 1 how the multiple-**Q** charge ordering model and single-**Q** charge ordering scenarios, while close

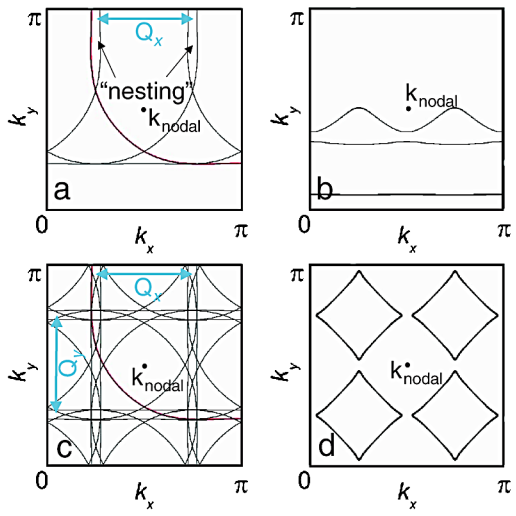

FIG. 1 (color online). (a) Quadrant of the unreconstructed FS (red) together with its translation by multiples of $\mathbf{Q}_x$ (black) for $\delta = 8\%$. (b) Open sheets that result for $V/W = 0.1$. (c) The same quadrant of the unreconstructed BZ together with its translation by multiples of $\mathbf{Q}_x$ and $\mathbf{Q}_y$. (d) An example showing how $V/W = 0.15$ leads to an electron pocket.

in energy [12], lead to profoundly different electronic structures. If one considers the single-$\mathbf{Q}$ Hamiltonian

$$H_1 = \begin{pmatrix} \varepsilon & V & 0 & V \\ V & \varepsilon_{\mathbf{Q}_x} & V & 0 \\ 0 & V & \varepsilon_{2\mathbf{Q}_x} & V \\ V & 0 & V & \varepsilon_{3\mathbf{Q}_x} \end{pmatrix}, \quad (1)$$

for example, in which V is the coupling and $\varepsilon_{\mathbf{Q}x}$ represents the electronic dispersion $\varepsilon(\mathbf{k})$ [23,24] translated by $\mathbf{Q}_x = [\frac{\pi}{2}, 0]$ [6], then susceptibility to gap formation (or approximate FS "nesting") is realized only near $\mathbf{k} = [0, \pi \pm \frac{\pi}{4}]$ in the extended BZ: not $\mathbf{k} = [\pi \pm \frac{\pi}{4}, 0]$ [see Fig. 1(a)]. Diagonalization of H_1 yields open FS sheets [see Fig. 1(b)]. In contrast, on considering simultaneous translations by $\mathbf{Q}_x$ and $\mathbf{Q}_y$, gap formation can occur at both $\mathbf{k} = [\pi \pm \frac{\pi}{4}, 0]$ and $(0, \pi \pm \frac{\pi}{4})$ [see Fig. 1(c)]. The open sheets of the single-$\mathbf{Q}$ model give way to a small FS pocket in Fig. 1(d) (on introducing V), necessary to produce quantum oscillations [1,2].

To construct a multiple-$\mathbf{Q}$ ordering Hamiltonian, we consider all possible translations $\mathbf{k} \rightarrow \mathbf{k} + m\mathbf{Q}_x + n\mathbf{Q}_y$ in which m and n are integers to arrive at

$$H_2 = \begin{pmatrix} \varepsilon & V & V_{\mathrm{II}} & V & V & V' & \cdots \\ V & \varepsilon_{\mathbf{Q}_x} & V & V_{\mathrm{II}} & V' & V & \cdots \\ V_{\mathrm{II}} & V & \varepsilon_{2\mathbf{Q}_x} & V & 0 & V' & \cdots \\ V & V_{\mathrm{II}} & V & \varepsilon_{3\mathbf{Q}_x} & V' & 0 & \cdots \\ V & V' & 0 & V' & \varepsilon_{\mathbf{Q}_y} & V & \cdots \\ V' & V & V' & 0 & V & \varepsilon_{\mathbf{Q}_y+\mathbf{Q}_x} & \cdots \\ \vdots & \vdots & \vdots & \vdots & \vdots & \vdots & \ddots \end{pmatrix}. \quad (2)$$

We initially neglect higher order terms (i.e., $V' = V_{\mathrm{II}} = 0$), consider V to be uniform, and neglect a possible component of $\mathbf{Q}$ orthogonal to the layers—similar FS results being envisaged [25] for multiple-$\mathbf{Q}$ d-density-wave order [26] or charge stripes that alternate on consecutive layers [18]. We further consider the commensurate case where $a = b = \pm\frac{1}{4}$ (relevant to many STM and neutron diffraction experiments), which yields a 16×16 matrix and 16 bands upon diagonalization.

Despite $\mathbf{k}_{\mathrm{nodal}} = [\pm\frac{\pi}{2}, \pm\frac{\pi}{2}]$ having 4 equivalent locations in the extended BZ, multiple-$\mathbf{Q}$ ordering folds these onto a single point in the reconstructed BZ yielding a concentration only of holes. The small size of the reconstructed BZ causes this hole surface area (corresponding to a frequency in the range $900 < F_h = \frac{\hbar A_h}{2\pi e} < 1400$ T, where A_h is the k-space area) to exceed 50% of the BZ area ($F_{\mathrm{BZ}} = \frac{\hbar A_{\mathrm{BZ}}}{2\pi e} \approx 1700$ T) for nominal hole dopings (in the range $8 \lesssim \delta \lesssim 11\%$) applicable to quantum oscillation experiments [1,2] [see Fig. 1(d)]. Band filling thus causes an electron pocket ($F_e = F_{\mathrm{BZ}} - F_h$) to become a protected feature of multiple-$\mathbf{Q}$ ordering.

FSs calculated for different combinations of δ and ratios V/W of V to the electronic bandwidth W [23] are shown in Fig. 2. The complexity of the FS obtained at weaker couplings ($V/W < 0.15$) in Fig. 2 originates from the combined effects of imperfect nesting and our neglect of the next nearest coupling V' between FSs translated by $\mathbf{Q}_x \pm \mathbf{Q}_y$. These "nest" almost as well [see Fig. 1(c)] as those with a relative translation of $\mathbf{Q}_x$ or $\mathbf{Q}_y$. On including V' in Figs. 3(a)–3(c), a simple electron pocket is obtained for weaker coupling strengths. Finally, in Figs. 3(d)–3(f), we include the effect of the ortho-II ordering potential V_{II}, which breaks the rotational symmetry of the FS. For the case considered ($V'/V = 0.6$ and $V/W = 0.05$), the electron pocket remains intact provided $V_{\mathrm{II}}/V \leq 0.4$.

We compare features of the calculated FSs in Figs. 2 (for $V/W \sim 0.15$) and 3 (for $V/W \sim 0.05$) with observed magnetic quantum oscillations in underdoped $YBa_2Cu_3O_{6+x}$—a single carrier type of pocket unaccompanied by a significant reservoir being indicated by the observation of chemical potential quantum oscillations [13]. Both the frequency $F \approx 500$ T and effective mass $m^* \approx 1$–$2m_e$ of the largest section obtained within the multiple-$\mathbf{Q}$ model we propose are close to those in experiments [1–4]—no adjustment having been made to the tight-binding representation of the dispersion obtained from band structure calculations [23,24]. As opposed to previously proposed single-$\mathbf{Q}$ models in which two nodal hole pockets are contained in each bilayer BZ, the small size of the BZ in the multiple-$\mathbf{Q}$ model we propose here causes it to contain only a single dominant electron pocket, yielding values for the Sommerfeld coefficient $\gamma_{\mathrm{model}} \approx 5$–$9$ mJ mol^{-1}K^{-2} (considering $V/W = 0.15$ and counting 2 bilayers) comparable to that $\gamma_{\mathrm{exp}} \approx 5.3$ mJ mol^{-1}K^{-2} obtained in heat capacity studies in strong magnetic fields [11]. The upper end of this range is caused by proximity to

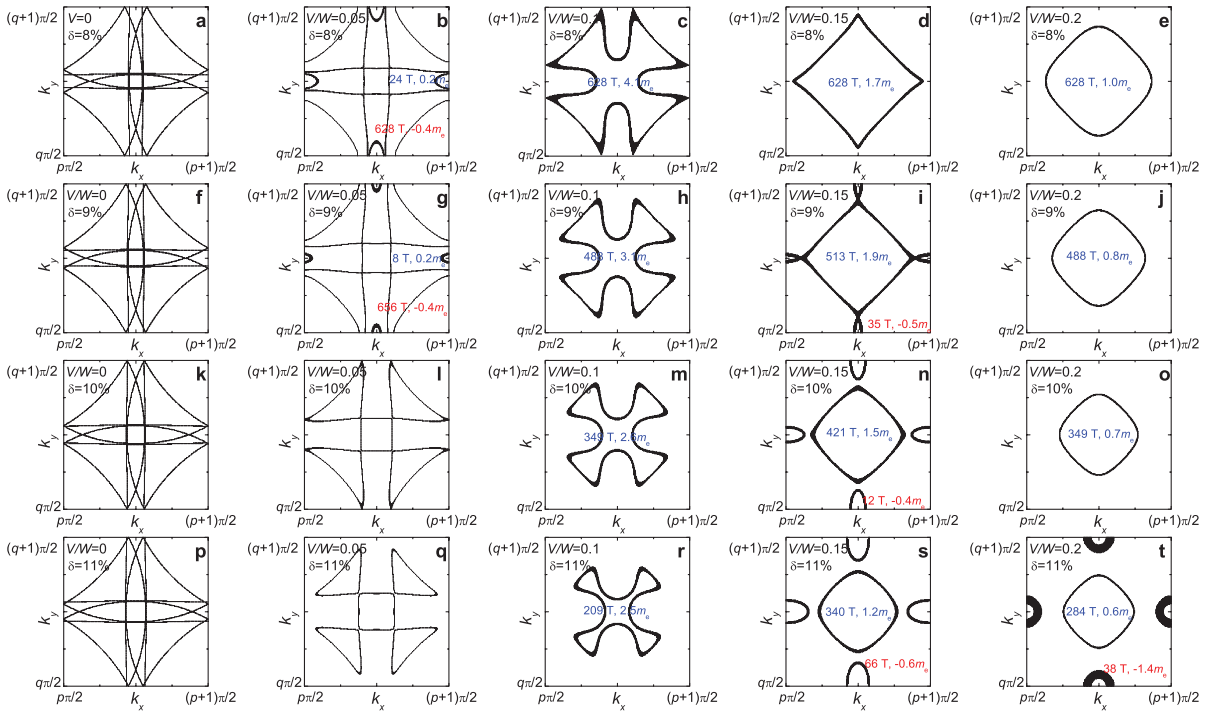

FIG. 2 (color online). The reconstructed FS according to Eq. (2) for $a = b = \pm\frac{1}{4}$, different ratios V/W, and effective hole doping δ as indicated (assuming $V' = V_{\mathrm{II}} = 0$). Also shown are the corresponding magnetic quantum oscillation frequencies according to Onsager's equation $F = A_k\hbar/2\pi e$ (where A_k is the FS cross section) and the corresponding band masses, where m_e is the free electron mass and a negative sign indicates holes. Line thicknesses are proportional to the inverse Fermi velocity.

a Lifshitz transition at $\delta \lesssim 9\%$ in the model. Furthermore, the electron character of the largest predicted pocket over a broad range of dopings and couplings (being the only pocket for many combinations of V and δ) yields negative Hall and Seebeck coefficients, as seen in strong magnetic fields in underdoped $YBa_2Cu_3O_{6+x}$ [2]. The crossover to the positive Hall effect observed at elevated temperatures [2] could potentially be caused by loss of order [21].

Features of the multiple-**Q** model are also compared with ARPES (and STM) FS measurements. Since the predicted electron pocket is constructed entirely from the nodal regions of $\varepsilon(\mathbf{k})$ and is also the largest pocket, the observation of Fermi arcs [7–9] would not be unexpected in this scenario. Specifically, as a consequence of coherence factors [27] and short correlation lengths [28], ARPES experiments may be expected to be sensitive chiefly to the portions of the reconstructed FS (black lines in Fig. 4) that overlap with the unreconstructed FS (depicted in gray).

In view of the FS comprising a single quasi-two-dimensional pocket identified in recent quantum oscillation experiments [13], the observed larger frequency [3] requires an additional explanation. The model we propose here offers some potential routes to explain the origin of such a larger frequency. Among these are magnetic breakdown frequencies resulting from tunneling across gaps in the FS—for instance, a BZ frequency F_{BZ} [29]. A complete understanding of these effects, however, is complicated by the fact that the magnetization experiments are performed in the vortex state [3]. Magnetic breakdown (and the Hall effect) will also be sensitive to topological details, such as interlayer tunneling, bilayer coupling [30], V, and the possible presence of small hole pockets. The small hole pockets in Fig. 2 are connected to the electron pocket via a quadratic band contact point, while in Fig. 3 they are connected via a Dirac point situated at $\delta = \frac{1}{8}$.

In summary, we identify an electron pocket located at the nodal regions of the BZ as a universal feature

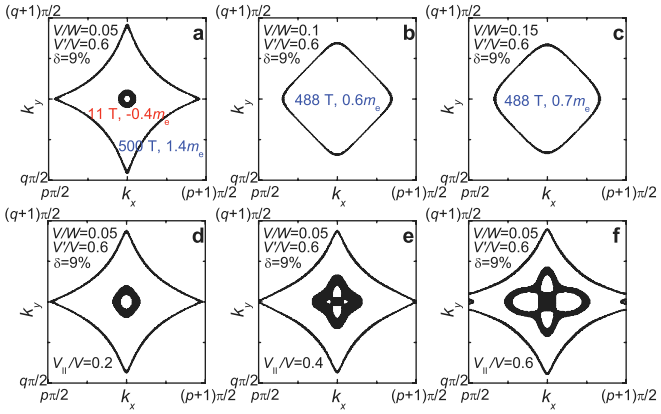

FIG. 3 (color online). (a)–(c) Reconstructed FS according to Eq. (2) for $a = b = \pm\frac{1}{4}$ and different values of the ratio V/W as indicated for an effective hole doping $\delta = 9\%$ with $V'/V = 0.6$ and $V_{\mathrm{II}} = 0$. (d)–(f) The same as (a) but with the effect of different ortho-II potentials (V_{II}) included.

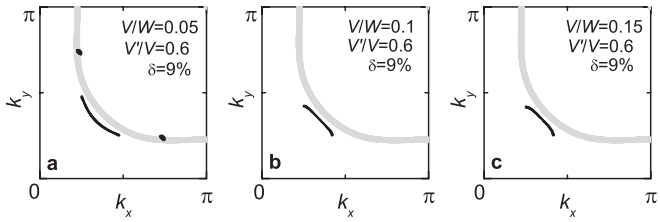

FIG. 4. The result of "unfolding" the reconstructed FSs in Figs. 3(a)–3(c) so as to trace the origin of the FS segments to the original BZ (1/4 of which is shown).

of multiple-**Q** charge ordering. A viable alternative is proposed to the previously proposed spin and/or charge models which lead to a combination of hole pockets at the nodes, electron pockets at the antinodes, and open sheets of FS. The applicability of this model to underdoped $YBa_2Cu_3O_{6+x}$ in which small FS pockets have been observed is particularly relevant given the recent discovery of charge order at high magnetic fields [21]—the size, location, and carrier type of the FS topology expected within this model are shown to be better consistent with experimental observations than previously proposed single-**Q** models. A further strength of the multiple-**Q** model is that the electron pocket is formed from the highest of the lower 8 bands in the multiple-**Q** model (out of a total 16 bands), suggesting that this pocket will remain robust against the introduction of a strong Coulomb repulsion in the model.

We acknowledge DOE BES project "Science at 100 Tesla" and helpful advice from G. G. Lonzarich.

[1] N. Doiron-Leyraud *et al.*, Nature (London) **447**, 565 (2007); A. Audouard *et al.*, Phys. Rev. Lett. **103**, 157003 (2009); S. E. Sebastian *et al.*, Proc. Natl. Acad. Sci. U.S.A. **107**, 6175 (2010).
[2] D. LeBoeuf *et al.*, Nature (London) **450**, 533 (2007); D. LeBoeuf *et al.*, Phys. Rev. B **83**, 054506 (2011); F. Laliberté *et al.*, arXiv:1102.0984.
[3] S. E. Sebastian *et al.*, Nature (London) **454**, 200 (2008); S. E. Sebastian *et al.*, Phys. Rev. B **81**, 214524 (2010).
[4] B. J. Ramshaw *et al.*, Nature Phys. **7**, 234 (2010); S. E. Sebastian, arXiv:1103.4178.
[5] M. R. Norman, Physics **3**, 86 (2010).
[6] A. J. Millis and M. R. Norman, Phys. Rev. B **76**, 220503 (2007); S. Chakravarty and H. Y. Kee, Proc. Natl. Acad. Sci. U.S.A. **105**, 8835 (2008).
[7] K. M. Shen *et al.*, Science **307**, 901 (2005).
[8] M. A. Hossain *et al.*, Nature Phys. **4**, 527 (2008); A. Kanigel *et al.*, Nature Phys. **2**, 447 (2006); H. Ding *et al.*, Nature (London) **382**, 51 (1996); A. Damascelli, Z. Hussain, and Z. X. Shen, Rev. Mod. Phys. **75**, 473 (2003); T. Valla *et al.*, Science **314**, 1914 (2006); J. Chang *et al.*, New J. Phys. **10**, 103016 (2008).
[9] J. Lee *et al.*, Science **325**, 1099 (2009).
[10] J. M. Tranquada *et al.*, Phys. Rev. B **81**, 060506 (2010); A. D. LaForge *et al.*, Phys. Rev. B **81**, 064510 (2010).
[11] S. C. Riggs *et al.*, Nature Phys. **7**, 332 (2011).
[12] A. Melikyan and M. R. Norman, arXiv:1102.5443.
[13] S. E. Sebastian *et al.*, arXiv:1103.4180.
[14] J. M. Tranquada *et al.*, Nature (London) **375**, 561 (1995); M. Fujita *et al.*, Phys. Rev. Lett. **88**, 167008 (2002); J. M. Tranquada *et al.*, Phys. Rev. B **54**, 7489 (1996).
[15] J. E. Hoffman *et al.*, Science **295**, 466 (2002); T. Hanaguri *et al.*, Nature (London) **430**, 1001 (2004).
[16] K. McElroy *et al.*, Phys. Rev. Lett. **94**, 197005 (2005); W. D. Wise *et al.*, Nature Phys. **4**, 696 (2008); M. Hashimoto *et al.*, Nature Phys. **6**, 414 (2010).
[17] J. A. Robertson *et al.*, Phys. Rev. B **74**, 134507 (2006).
[18] M. V. Zimmermann *et al.* Europhys. Lett. **41**, 629 (1998); R. S. Markiewicz, Phys. Rev. B **71**, 220504 (2005); N. B. Christensen *et al.*, Phys. Rev. Lett. **98**, 197003 (2007).
[19] Multiple-**Q** spin ordering with $\mathbf{Q}_s = [\pi(1 \pm \frac{1}{4}), \pi]$ and $[\pi, \pi(1 \pm \frac{1}{4})]$ is expected to yield a charge Bragg peak at $\mathbf{Q} = [\pm\pi/4, \pm\pi/4]$. Its absence could support either unidirectional spin stripe domains [17] or multiple-**Q** charge ordering without concomitant spin order.
[20] D. Haug *et al.*, New J. Phys. **12**, 105006 (2010).
[21] M.-H. Julien, in Proceedings of the Aspen Winter Conference, 2011 (unpublished).
[22] X. Liu *et al.*, Phys. Rev. B **78**, 134526 (2008).
[23] We use $\varepsilon = \varepsilon_0 + 2t_{10}[\cos ak_x + \cos bk_y] + 2t_{11}[\cos(ak_x + bk_y) + \cos(ak_x - bk_y)] + 2t_{20}[\cos 2ak_x + \cos 2bk_y]$ [24], with bandwidth $W = 8t_{10} = 3$ eV and next nearest neighbor hoppings $t_{11}/t_{10} = -0.32$ and $t_{20}/t_{10} = 0.16$. The chemical potential is adjusted for each calculation to ensure compatibility with Luttinger's theorem.
[24] O. K. Andersen *et al.*, Phys. Chem. Solids **56**, 1573 (1995).
[25] The nodal arc section of the FS is only weakly affected by the vanishing of V at the nodes [26], while stripes alternating on consecutive layers [18] introduce an additional periodicity in the interlayer direction—minimally impacting the in-plane topology.
[26] K. Seo, H.-D. Chen, and J. Hu, Phys. Rev. B **76**, 020511 (2007).
[27] J.-X. Li, C.-Q. Wu, and D.-H. Lee, Phys. Rev. B **74**, 184515 (2006).
[28] N. Harrison, R. D. McDonald, and J. Singleton, Phys. Rev. Lett. **99**, 206406 (2007).
[29] Mg provides an example of a simple metal exhibiting magnetic breakdown and a BZ frequency in the magnetic susceptibility; J. W. Eddy, Jr. and R. W. Stark, Phys. Rev. Lett. **48**, 275 (1982).
[30] Coupling between and within bonding and antibonding bands will yield a doubly degenerate frequency F_e and split frequencies $F_e \pm \Delta F$, respectively, where ΔF reflects the magnitude of the bilayer splitting at the nodes.